

Study of ${}^7\text{Li}$ elastic scattering and the lithium-induced reaction of one-nucleon transfers from ${}^{10}\text{B}({}^7\text{Li}, {}^6\text{Li}){}^{11}\text{B}^*$

Sergey Stukalov,¹ Yuri Sobolev,^{1,2,†} Yuri Penionzhkevich,^{1,3} Nassurlla Burtebayev,^{4,5} Sergey Goncharov,^{6,‡} Yuri Gurov,^{1,3} Andrey Danilov,² Alla Demyanova,² Maulen Nassurlla,^{4,5} Viktor Starastin,^{2,3} Alexey Shakhov,¹ Semyon Raidun,² and Nguyen Hoai Chau^{1,7}

¹Joint Institute for Nuclear Research, Dubna, Moscow Region 141980, Russia

²National Research Centre Kurchatov Institute, Moscow 123182, Russia

³National Research Nuclear University MEPhI, Moscow 115409, Russia

⁴Institute of Nuclear Physics of the Ministry of Energy of the Republic of Kazakhstan, Almaty 050032, Republic of Kazakhstan

⁵Al-Farabi National University, Almaty 050032, Republic of Kazakhstan

⁶M.V. Lomonosov Moscow State University, Moscow 119991, Russia

⁷Institute for Science and Technology of Energy and Environment, Hanoi 122000, Vietnam

The angular distributions of elastic scattering of ${}^7\text{Li}$, as well as the lithium-induced reaction of one-nucleon transfers ${}^{10}\text{B}({}^7\text{Li}, {}^6\text{Li}){}^{11}\text{B}$ were measured at $E_{\text{lab}} = 58$ MeV. Experiment was done using U-400 accelerator beam of the FLNR JINR, Dubna. Angular distribution for reaction ${}^{10}\text{B}({}^7\text{Li}, {}^6\text{Li}){}^{11}\text{B}$ with excitation of the 3.56 MeV state (${}^6\text{Li}^*$) is present for the first time. The DWBA analysis of the differential cross section of the ${}^{10}\text{B}({}^7\text{Li}, {}^6\text{Li}){}^{11}\text{B}$ ground state (g.s.) transition and excited ($J^\pi = 0^+$, $T = 1$, $E = 3.56$ MeV) state of ${}^6\text{Li}$ transition was performed. The optical model potentials were obtained by fitting of measured elastic scattering data and evaluating parameters for the output reaction channels. Phenomenological approaching based on solving an approximate equation for the reaction form factor was used to determine its radial dependence and empirical values of asymptotic normalization coefficient (ANC). Obtained values of ANC's for the ${}^6\text{Li}_{\text{g.s.}}$ and ${}^6\text{Li}^*(3.56$ MeV) states are similar to literature one. Comparison of the radial dependences of form factors shows that the wave function of the ${}^6\text{Li}$ nucleus in excited ($J^\pi = 0^+$, $T = 1$, $E = 3.56$ MeV) state has increased spatial dimension compared to the ground state, and in both cases some larger spatial size than the ground states of the ${}^{11}\text{B}$ and ${}^{10}\text{B}$. Within the framework of our analysis, we can confirm that the radius of the ${}^6\text{Li}$ nucleus in the 3.56 MeV state is larger than in the ground state. This result is an argument in favor of a halo existence in ${}^6\text{Li}^*(3.56$ MeV) state, while the question of a halo in ${}^6\text{Li}_{\text{g.s.}}$ still leaves open.

Keywords: elastic scattering, optical potentials, transfer reactions, asymptotic normalization coefficient, exotic isobar analog states, two nucleon halo, increased radius

I. INTRODUCTION

Experimental studies of the properties of neutron-rich radioactive nuclei located far from the stability line led to the discovery of a new nuclear structure in some nuclei (${}^6\text{He}$, ${}^{11}\text{Li}$) - a neutron halo [1]. According to modern concepts, such nuclei consist of a dense nuclear core and a low-density outer region formed by valence weakly bound neutrons. Initially, the term "exotic nuclei" itself referred to these nuclei. One of the main manifestations of properties of halo is an increased radius of the valence nucleons density distributions, 2-3 times greater than the size of the core.

Among nuclei with a two-neutron halo [2], the so-called Borromean structure is quite common - a system, in which each pair of the three participants does not form a bound state, while all three participants form a bound nuclear system that is stable with respect to neutron emission (for example, ${}^4\text{He}+n+n$ and ${}^9\text{Li}+n+n$ in the nuclei of ${}^6\text{He}$ and ${}^{11}\text{Li}$, respectively).

One of the most interesting issues in the study of exotic nuclei is the problem of preserving the properties of the halo

in excited states of nuclei that are isobaric analogues of the ground states of nuclei with a halo. From this point of view, one of the interesting objects, most accessible for experimental study, is the stable nucleus ${}^6\text{Li}$, which, together with the nuclei ${}^6\text{He}$ and ${}^6\text{Be}$, forms an isobaric triplet $A = 6$.

The ground state of the ${}^6\text{Li}$ nucleus, according to the hypothesis proposed in [3–6], has a "tango structure", i.e. a quasi-molecular structure " α -core" - "deuteron" in which p and n valence nucleons move in a correlated manner in the deuteron, without forming $\alpha+p$ and $\alpha+n$ bound states with the " α -core".

An argument in favor of this hypothesis can be the energy dependence of the total cross sections $\sigma_R(E)$ of the reactions ${}^6\text{He}, {}^6,7\text{Li}+{}^{28}\text{Si}$ [7, 8], measured at $E_{\text{LAB}} = (7 \div 20)$ AMeV, which showed that the values of $\sigma_R({}^6\text{He}, {}^6\text{Li}+{}^{28}\text{Si})$ exceed the cross sections of the reactions ${}^7\text{Li}+{}^{28}\text{Si}$.

An additional argument for the presence of a halo structure in the ground state of ${}^6\text{Li}$ can also be the widths of the momentum distributions of ${}^4\text{He}$ during the breakup of ${}^6\text{He}$ and ${}^6\text{Li}$ nuclei [9]. The width of the momentum distribution of ${}^4\text{He}$ formed in the breakup reaction of ${}^6\text{Li}$ was $\sigma \sim 50$ MeV/c [9] and occupied an intermediate value between the widths of the ${}^4\text{He}$ distributions $\sigma \sim 28$ MeV/c and $\sigma \sim 100$ MeV/c obtained in the breakup reactions of ${}^6\text{He}$ and stable nuclei, respectively.

To date, experimental data on the spatial structure of the excited state of ${}^6\text{Li}$ ($J^\pi = 0^+$, $T = 1$, $E = 3.56$ MeV), which

* The research was funded by the Russian Science Foundation (project № 24-22-00117) and by the NRC "Kurchatov Institute"

† Corresponding author 1, Yuri Sobolev, sobolev@jinr.ru

‡ Corresponding author 2, Sergey Goncharov, gsa@srd.sinp.msu.ru

is an isobaric analog of ${}^6\text{He}$ g.s., are limited. Most of the studies [10–14], investigated multi-step reaction channels, (t , p), charge exchange ${}^1\text{H}({}^6\text{He}, {}^6\text{Li})n$, etc. Analysis of multi-step reaction channels requires consideration of a larger number of possible combinations [14], which complicates obtaining unambiguous results, in contrast to stripping and pickup reactions.

Based on the results of the study of the charge exchange reaction ${}^1\text{H}({}^6\text{He}, {}^6\text{Li})n$ [10–13], a conclusion was made about the two-nucleon halo structure of the state ${}^6\text{Li}$ ($J^\pi = 0^+$, $T = 1$, $E = 3.56$ MeV), similar to ${}^6\text{He}_{\text{g.s.}}$. Also in the work [15] a comparison of the *rms*-radii of the ground (${}^6\text{He}$) and excited (${}^6\text{Li}^*$) isobar-analog states was carried out, based on the analysis of differential cross sections obtained in different experiments. An estimate of the *rms*-radius of the state ${}^6\text{Li}$ ($J^\pi = 0^+$, $T = 1$, $E = 3.56$ MeV) [15] was made within the framework of the Modified Diffraction Model method [16] in the analysis of the angular distributions of the cross sections of elastic and inelastic scattering of ${}^3\text{He}+{}^6\text{Li}$ [17]. The obtained radius, within the error limits, coincided with the calculations within the *ab initio* NCSM (no-core shell model) [18]. Moreover, the calculations [18] showed that the radius of the ground state of ${}^6\text{Li}$, within the error limits, coincides with the radius of the 3.56 MeV state of ${}^6\text{Li}$.

At present, there are insufficient experimental data to draw an unambiguous conclusion about the spatial structure of ${}^6\text{Li}_{\text{g.s.}}$. Experimental values of the matter radius of ${}^6\text{Li}_{\text{g.s.}}$ vary significantly within the range from $r_m = 2.09 \pm 0.02$ fm [19] to $r_m = 2.45 \pm 0.07$ fm [20].

It should be noted that until now there were no experimental results on direct transfer reactions, on base of which *rms*-radii of ${}^6\text{Li}_{\text{g.s.}}$ and excited state of ${}^6\text{Li}$ ($J^\pi = 0^+$, $T = 1$, $E = 3.56$ MeV) (the isobaric-analog state of ${}^6\text{He}_{\text{g.s.}}$) can be obtained simultaneously.

The aim of this work is the simultaneous measurement of angular distributions of differential cross sections of the transfer reaction ${}^{10}\text{B}({}^7\text{Li}, {}^6\text{Li}){}^{11}\text{B}$ with transition to the ground ${}^6\text{Li}_{\text{g.s.}}$ and excited ${}^6\text{Li}$ ($J^\pi = 0^+$, $T = 1$, $E = 3.56$ MeV) states together with channels of elastic scattering ${}^7\text{Li}+{}^{10}\text{B}$ and, based on the analysis of these data, to obtain information about the spatial structure of the ${}^6\text{Li}$ nucleus states, and the some quantitative characteristic nature of the interaction of the neutron with the ${}^6\text{Li}$ nucleus in these states.

II. EXPERIMENTAL SETUP

Measurement of angular distributions of differential cross sections of ${}^7\text{Li}+{}^{10}\text{B}$ reaction products was performed using the U-400 cyclotron of the JINR Laboratory of Nuclear Reactions, Dubna. Fig. 1 shows the block diagram of the experimental setup elements. The ${}^7\text{Li}$ ion beam with energy $E = 58$ MeV and energy resolution $\Delta E_{\text{(FWHM)}} = 0.5$ MeV was focused using a system of magnets in the ion guide channel, a position-sensitive multiwire “X-Y” chamber, and was formed by diaphragms D1-D4, which formed a beam collimator (see Fig. 1). The beam formed by the collimator in the target position M had a beam spot diameter $\varnothing = 3.6$ mm and an angular

aperture of $\Delta\Theta \approx 0.2^\circ$.

A self-supporting target of the isotope ${}^{10}\text{B}$ ($t \approx 0.05$ mg/cm², $\varnothing = 1.0$ cm), containing impurities of the isotopes ${}^{12}\text{C}$ (9%) and ${}^{16}\text{O}$ (6%), was installed in the center of the reaction chamber perpendicular to the beam axis.

The impurities were estimated using known experimental data on elastic scattering in the reactions ${}^7\text{Li}+{}^{10}\text{B}$ [21], ${}^7\text{Li}+{}^{12}\text{C}$ [22], ${}^7\text{Li}+{}^{16}\text{O}$ [22] at close energies ($E_{\text{lab}} = 36$ MeV and 39 MeV).

At a distance of 30 cm from the target M in beam direction a Faraday cup F.C. was located. (Fig. 1), which is a thick-walled (~ 0.5 cm) steel pipe with a diameter of 4 cm and a height of 25 cm. The beam current data measured by Faraday cup and the beam integrator unit (ORTEC – 439) was recorded together with the experimental data by the data acquisition system (DAQ).

Additional control of the beam and the state of the target M was carried out using a monitor E Si(Li)-detector (not shown in Fig. 1).

The DAQ of the experimental setup consisted of the VME electronics units (MVLC crate controller [23], MADC-32 ADC [23]) and NIM standard logical units and operated by MVME Mesytec program [23].

The DAQ master trigger was the MVLC VME block, to the input of which signals of a request to record an event were received from any of the detectors of the setup, as well as pulses from the beam current integrator unit. The DAQ dead time values were estimated by the number of MVLC input request pulses and the number of events written to files. The DAQ system was used to measure the angular distributions of the differential cross sections of the reaction products, which were recorded using two detector groups (see Fig. 1). Each detector group consisted of four $\Delta E - E$ telescopes of Si detectors. The first group consisted of 100 μm thick ΔE detectors and 3000 μm thick E Si(Li) detectors and was used to measure particles emitted in the forward angles ($7^\circ < \Theta < 30^\circ$). The second group consisted of 30 μm and 800 μm thick ΔE and E detectors for reaction product measurements at $\Theta > 20^\circ$.

In front of each telescope, there were lead diaphragms of square cross section $\sim 3 \times 4$ mm², providing a solid angle of the detectors of the telescopes of the first and second groups $\Omega = 1.3 \times 10^{-4}$ sr and 2.2×10^{-4} sr, respectively.

The angular distance $\Delta\Theta_{\text{LAB}}$ between neighboring telescopes of the first and second groups is $\Delta\Theta_{\text{LAB}} = 3.2^\circ$ and 1.7° , respectively. The Θ_{LAB} telescope angles were varied with an accuracy of $\pm 0.50^\circ$. The energy resolution of the ΔE and E detectors of the telescopes was no worse than $\Delta E = 60$ keV (${}^{226}\text{Ra}$ α -source). Fig. 2 shows the two-dimensional $\Delta E \times E$ spectrum of the ${}^7\text{Li}+{}^{10}\text{B}$ reaction products in one of the 8 ΔE - E telescopes.

Fig. 3 shows the energy spectrum of ${}^6\text{Li}$ recorded by the telescope located at $\Theta_{\text{LAB}} = 10^\circ$. The total ($\Delta E + E$) energy of ionization losses of ${}^6\text{Li}$ in the ΔE and E detectors of the telescope in MeV units is plotted along the abscissa axis. The number of events per 100 keV of the abscissa scale is plotted along the ordinate axis.

In Fig. 3 the positions of the peaks of the ground and ex-

cited states of the nuclei ${}^6\text{Li}$, ${}^{11}\text{B}$, as well as ${}^{13}\text{C}$, ${}^{17}\text{O}$, which are the products of reactions on the nuclei ${}^{12}\text{C}$, ${}^{16}\text{O}$, which constitute impurities in the target, are indicated by vertical arrows with corresponding caption.

The differential cross sections of elastic scattering of ${}^7\text{Li}$ on the ${}^{10}\text{B}$ target at the beam energy $E_{\text{LAB}}=58$ MeV are shown in Fig. 4 by filled squares.

The differential cross sections of the reaction channels of transfer of ${}^{10}\text{B}({}^7\text{Li}, {}^6\text{Li}){}^{11}\text{B}$ to the ground and excited ${}^6\text{Li}(J^\pi = 0^+, T = 1, E = 3.56 \text{ MeV})$ states of the ${}^6\text{Li}$ nucleus are shown in Fig. 4 by filled triangles and circles, respectively.

Obtained angular distributions were analyzed within Distorted Wave Born Approximation (DWBA).

III. THEORY

Direct nuclear reactions in most cases are peripheral reactions. The largest contribution from the direct reaction to

the angular distribution occurs in the forward region of the angles, forming the so-called “main maximum”, which contains information about the interactions and structure of the participating nuclei. When analyzing angular distributions in the region where the main maximum of the direct transfer reaction can be observed, it seems quite adequate to use the “Distorted Wave Born Approximation” (DWBA) method [24]. The use of various structural models within the framework of this method makes it possible to obtain from such analysis information about features of the distribution of matter in the states of nuclei under study and quantities characterizing the interaction of a neutron with a ${}^6\text{Li}$ in ${}^7\text{Li}$.

In DWBA, for the reaction $A(a,b)B$ caused by the interaction V , we have the expression for the transition amplitude (see, for example, [24]):

$$T_{\text{DWBA}} = \int u_b^{(-)*}(k_b, r_b) \langle \Psi_b \Psi_B | |V| | \Psi_a \Psi_A \rangle u_a^{(+)}(k_a, r_a) dr_a dr_b \quad (1)$$

u_i – “distorted waves” – wave functions that describe elastic scattering in the input and output channels of the reaction, satisfying the corresponding asymptotic conditions at large distances.

Elastic scattering in this case involves taking into account

the loss of flux through many other reaction channels (including the compound nucleus), none of which is the most important. These channels are represented on average using a complex optical potential (OP), which is here constructed within the phenomenological approach, using the usual Woods-Saxon parameterization:

$$U(r) = -Vf(x_V) - iW_S f(x_S) + i4W_D \frac{df(x_D)}{dx_D} + V_C(r) \quad (2)$$

$$f(x) = (e^x + 1)^{-1} \quad x_i = (r_i - R_i)/a_i \quad R_i = r_i A^{1/3} \quad (i = V, S, D) \quad (3)$$

The Coulomb potential $V_C(r)$ is modeled by the potential of interaction of a point charge Z_{ae} with a uniformly charged sphere having a charge Z_{Ae} and a radius R_C , which can be

estimated through the root-mean-square charge radii of the nuclei. When nuclear spins are not zero, a spin-orbit potential is added:

$$V_{\text{SO}}(r) = (V_{\text{SO}} + iW_{\text{SO}}) \left(\frac{\hbar}{m_\pi c} \right)^2 \frac{1}{r} \frac{df(x_{\text{SO}})}{dr} (L \cdot I_a) \quad (4)$$

The parameters are selected to describe the observed elastic scattering in a given channel at the appropriate energy, if such data are available. To be confident in the correctness of the description of elastic scattering in cases where such data are not available, additional empirical information is used on

the energy and mass systematic of integral characteristics, for example, reaction cross sections and volume integrals of OP components. As initial one the parameters of the so-called “global potentials” can be used. These parameters as the functions of energy, charges and mass numbers were deter-

mined as a result of the analysis of a very large set of experimental data for a given projectile nucleus in a wide range of energies and target nuclei, or for a narrower mass region, for example, $1p$ -shell nuclei.

In the DWBA amplitude (1), the matrix element is the overlap integral of the interaction V and the wave functions of the interacting nuclei (a, A) and product nuclei (b, B) that contains all the structural information. Separation of radial and angular variables through expansion in transferred angular momentum (see, for example, [24]) identifies the product of the radial parts of the overlap integrals for the so-called “light” ($a = b + n$) and “heavy” ($B = A + n$) systems, often called the corresponding “cluster form factors” or “reaction form factors” $I_{lsj}^{ab}(r)$ and $I_{lsj}^{BA}(r)$, where lsj are the transferred orbital, spin and total momentum and r is the distance between the transferred particle n and the core $A(b)$. Note that in the theory, the spectroscopic factors (SF) S_{lsj}^{ab} and S_{lsj}^{BA} are determined as norm of corresponding form factor.

It is known (see, for example, [25]) that form factors can be represented as solutions to the inhomogeneous equation:

$$T_r - V_{lsj}^0(r) - \epsilon_{lsj} I_{lsj}(r) = P(r) \quad (5)$$

where T_r is the operator of the kinetic energy of the relative motion of the transferred particle and the core, $V_{lsj}^0(r)$ is the “self-consistent field” of interaction between the particle and the core, which alone serves as the source of this field, ϵ_{lsj} is the binding energy of the transferred particle in a given state of the nucleus $B(a)$. The right side of equation (4) is an integral operator, including residual interactions mixing different configurations and taking into account the Pauli principle for the transferred particle relative to the core.

There are various ways to determine form factors. Direct one is calculation overlap integrals using model nuclear wave functions. Other approaches involve an approximate solution of equation (4).

Here, to solve this equation, some phenomenological approach is used. The right side of equation (4) is replaced by some local operator acting directly on the form factor $P(r) = \Delta V_{lsj}(r) I_{lsj}(r)$. Moving this to the left side we get a homogeneous equation with some effective potential.

$$V_{lsj}(r) = V_{lsj}^0(r) + \Delta V_{lsj}(r) \quad (6)$$

$$(T_r - V_{lsj}(r) - \epsilon_{lsj}) I_{lsj}(r) = 0 \quad (7)$$

Due to the short action of these potentials, the boundary conditions at large distances are determined only by the binding energy ϵ_{lsj} , i.e. the asymptotic of the form factor is expressed by the spherical Hankel function (or the Whittaker function in the case of a charged particle)

$$I_{lsj}(r \rightarrow \infty) = N^{1/2} C_{lsj} \kappa h_l(i\kappa r) \quad (8)$$

$\kappa^2 = 2\mu\epsilon_{lsj}/\hbar^2$, μ – reduced mass, N – coefficient taking into account the antisymmetrization of wave functions.

The value of NC_{lsj} is called the asymptotic normalization coefficient (ANC), which is associated with the nuclear vertex constant (NVC) G_{lj} , which characterizes the interaction of the transferred particle with the core:

$$G_{lj}^2 = \pi(\hbar/\mu c)^2 NC_{lj}^2. \quad (9)$$

Due to direct nuclear reactions in most cases are peripheral reactions, the angular distributions are sensitive only to the surface (asymptotic) part of the reaction form factor. This allows us to obtain empirical values of NVC and ANC from the description of the main peak of the experimental angular distribution. However, this also prevents us from obtaining the SF, the determination of which requires knowledge of the form factor for all r . (For more details, see, for example [26, 27]).

Here, to determine the form factor, ANC and NVC, approximate equation (6) was solved for each configuration lsj with model potential $V_{lsj}(r)$ in a simple 3-parameter Woods-Saxon form.

$$V_{lsj}(r) = V(e^x + 1)^{-1}, \quad x = (r - R)/a \quad (10)$$

The parameters R and a of the model potential $V_{lsj}(r)$ are selected to best describe the shape of the angular distribution of the reaction at least near the region of the main maximum at the forward angles, and its depth V is determined for given R and a from the binding energy ϵ_{lsj} using the well depth fitting procedure. If the solution to equation (6) is determined normalized to 1, the ANC (and, accordingly, the NVC) is determined from normalization to the absolute value of the experimental cross section. Obviously, the accuracy of determining these quantities is due to measurement error of the absolute value of the experimental cross section. In our case, we estimate this error to be $\sim 15\%$.

As a result of such an analysis, we obtain radial dependences for the form factors and the ANC value, which can be compared both with the results of available theoretical calculations with model wave functions of nuclei, and with empirical values obtained from the analysis of other reactions. In particular, by comparing the form factors for different states of the nucleus of interest to us, we can obtain indirect information about the difference in the sizes of the nucleus in these states (see below).

The differential cross sections of elastic scattering and reaction were calculated using the code FRESKO [28], with coherent consideration of all allowed combinations of transferred angular momentum and spins lsj .

IV. RESULTS AND ANALYSIS

The optical potential in the input channel of ${}^7\text{Li}+{}^{10}\text{B}$ was constructed based on the analysis of our elastic scattering data at 58 MeV and the data from [21] at 39 MeV. In both cases, the same sets of geometric parameters (effective radii and diffuseness) and parameters of the spin-orbit and Coulomb potentials were recorded:

$$\begin{aligned}
r_R = 0.55 \text{ fm}, \quad a_R = 0.86 \text{ fm}, \quad r_S = 0.88 \text{ fm}, \quad a_S = 0.30 \text{ fm}, \quad r_D = 0.65 \text{ fm}, \quad a_D = 0.95 \text{ fm}, \\
r_C = 0.60 \text{ fm}, \quad V_{SO} = 6.0 \text{ MeV}, \quad r_{SO} = 0.55 \text{ fm}, \quad a_{SO} = 0.86 \text{ fm}
\end{aligned} \quad (11)$$

Here:

$$R_i = r_i(A_p^{1/3} + A_t^{1/3}), \quad (i = R, S, D, C, SO). \quad (12)$$

In this case, reasonable values and the trend of the energy dependence were obtained for the force parameters (potential depths), volume integrals and reaction cross sections (see Table 1). The description of the angular distributions is presented in Figure 5.

Table 1. Optical potentials in Woods-Saxon form (2)-(3) for ${}^6\text{Li}+{}^{10}\text{B}$

$E_{\text{LAB}},$ MeV	$V_r,$ MeV	$W_S,$ MeV	$W_D,$ MeV	$-J_V,$ MeV fm ³	$-J_W,$ MeV fm ³	$\sigma_r,$ mb
58.0	250.	10.0	22.0	415.	177.	1468.
39.0	290.	7.0	16.0	481.	128.	1434

Unfortunately, there are no experimental data on elastic scattering for the output channels ${}^6\text{Li}+{}^{11}\text{B}$ in the energy range of interest to us. However, there are data on scattering ${}^6\text{Li}+{}^{12}\text{C}$ [29–31] at 50, 54 and 59.8 MeV that can be relied upon. We tried to construct a kind of regional potential for the scattering of lithium nuclei on 1p-shell nuclei by fixing

the geometric parameters (10)-(11) and using these data. Table 2 presents the energy dependent parameters and integral characteristics obtained from the analysis of ${}^6\text{Li}+{}^{12}\text{C}$ data. Figure 6 shows the quality of description of the corresponding experimental angular distributions.

Table 2. Optical potentials in Woods-Saxon form (2)-(3) for ${}^6\text{Li}+{}^{12}\text{C}$

$E_{\text{LAB}},$ MeV	$V_r,$ MeV	$W_S,$ MeV	$W_D,$ MeV	$-J_V,$ MeV fm ³	$-J_W,$ MeV fm ³	$\sigma_r,$ mb
59.8	255.	14.0	19.5	419.	170.	1392.
54.0	270.	12.0	18.0	444.	154.	1385.
50.0	300.	10.0	16.0	493.	135.	1372.

Note that using a minimum number of variable parameters, it was possible to obtain the correct energy behavior of the potential characteristics and a fairly good description of the data in the region of forward angles.

Based on these parameters, we evaluated the parameters for the ${}^6\text{Li}+{}^{11}\text{B}$ output channels at real energies corresponding to the yield of the ${}^6\text{Li}$ nucleus in the ground and excited states. The parameters used for reaction calculations are given in Table 3.

Table 3. Optical potentials in Woods-Saxon form (2)-(3) for ${}^6\text{Li}+{}^{12}\text{C}$

	$E_{\text{LAB}},$ MeV	$V_r,$ MeV	$W_S,$ MeV	$W_D,$ MeV	$-J_V,$ MeV fm ³	$-J_W,$ MeV fm ³	$\sigma_r,$ mb
${}^6\text{Li}_{(\text{g.s.})} + {}^{11}\text{B}$	59.2	285.	13.0	17.0	496.	159.	1365.
${}^6\text{Li}^*(3.56) + {}^{11}\text{B}$	53.7	285.	12.0	16.0	496.	149.	1362.

Using the obtained optical potentials, we analyzed the measured differential cross sections of the reaction in two stages. First, to fix the form factor $\{{}^{11}\text{B}(3/2^-, T=1/2, \text{g.s.}), \text{n}^{10}\text{B}(3^+, T=0, \text{g.s.})\}$, we used the empirical form factor ${}^7\text{Li}(3/2^-, T=1/2, \text{g.s.}), \text{n}^6\text{Li}(1^+, T=0, \text{g.s.})$ recently obtained by a similar approach from the analysis of the ${}^7\text{Li}(d, t){}^6\text{Li}$ reaction at a deuteron energy of 14.5 MeV [32]. This form factor and its ANC are in good agreement with both the empirical form factor previously obtained from the analysis of the ${}^7\text{Li}(d, t){}^6\text{Li}$ reaction at a deuteron energy of 18 MeV [33] and the theoretical calculations [34] based on an approximate solution of the equation (4) for the form factor. Thus we have defined and recorded the values of the obtained model potential parameters and ANC for the form factor $\{{}^{11}\text{B}(3/2^-, T=1/2, \text{g.s.}), \text{n}^{10}\text{B}(3^+, T=0, \text{g.s.})\}$.

We also included in the consideration the data in the region of forward angles obtained in [35] at energy of 24 MeV for the ground state of ${}^6\text{Li}$. For ease of comparison, Figure 7 shows our data and the data from [35] and the DWBA calculation as a function of the transferred momentum in the region of forward angles.

Having thus fixed the form factor $\{{}^{11}\text{B}(3/2^-, T=1/2, \text{g.s.}), \text{n}^{10}\text{B}(3^+, T=0, \text{g.s.})\}$, we determined the parameters of the model potential, the radial form and the ANC of the form factor $\{{}^7\text{Li}(3/2^-, T=1/2, \text{g.s.}), \text{n}^6\text{Li}(0^+, T=1, 3.56)\}$ from the analysis of the measured differential cross sections in the channel with yield of the ${}^6\text{Li}$ in the excited state $0_1^+(3.56 \text{ MeV})$. The Figure 8 shows the angular distributions of the reaction (calculated and experimental) for the excited 3.56 MeV state of the ${}^6\text{Li}$ nucleus.

The values of the obtained model potential parameters and ANC and their comparison with the results of analysis and

theoretical calculations of other authors are presented in the Table 4.

Table 4. The values of the obtained model potential parameters and ANC

A+1(I^π, T, E^*), nA(I^π, T, E^*)	(l, j)	$-V$ MeV	R fm	a fm	$\langle r^2 \rangle^{1/2}$ fm	NC^2 fm $^{-1}$	NC_{theor}^2 fm $^{-1}$	NC_{exp}^2 fm $^{-1}$
${}^7\text{Li}(3/2^-, 1/2, \text{g.s.}), {}^6\text{Li}(1^+, 0, \text{g.s.})$	(1, 3/2) + (1, 1/2)	60.2	2.36	0.9	3.14	3.05(46)[32]	2.94[34]	3.17(53) [33]
${}^7\text{Li}(3/2^-, 1/2, \text{g.s.}), {}^6\text{Li}(0^+, 1, 3.56)$	(1, 3/2)	66.7	2.18	1.6	3.50	2.76(39)	2.47[34]	2.91(35) [33] 3.16(47) [32]
${}^{11}\text{B}(3/2^-, 1/2, \text{g.s.}), {}^{10}\text{B}(3^+, 0, \text{g.s.})$	(1, 3/2)	43.3	3.34	0.5	2.89	12.4(1.9)	13.1[34]	31.4(3.0) [33]

We note that the root-mean-square radius of the form factor $\{{}^7\text{Li}(3/2^-, T=1/2, \text{g.s.}), {}^6\text{Li}(0^+, T=1, 3.56)\}$ turned out to be larger than that for the ground state of ${}^6\text{Li}$. Figure 9 for all three form factors normalized to 1 shows a comparison of the radial dependences of the values $r^4 I_{lj}^2(r)$, which are the integrands in calculating the mean-square radii of these form factors. This figure demonstrates the difference in spatial dimensions of the wave function of the ${}^6\text{Li}$ in different states.

So, our results indirectly indicate that the wave function of the ${}^6\text{Li}$ nucleus in the $0^+, T = 1$ (3.56 MeV) state has increased spatial dimension compared to the ground state, and in both cases some larger spatial size than the ground states of the ${}^{11}\text{B}$ and ${}^{10}\text{B}$ nuclei. This means that radius of the g.s. of ${}^6\text{Li}$ is a little bit larger than radius of the ${}^{11}\text{B}$ and ${}^{10}\text{B}$ nuclei. Radius of the ${}^{11}\text{B}$ is ~ 2.3 fm. And radius of the 3.56 MeV state is even larger than the radius of the g.s. Note that this result is in some contradiction to results of ab initio calculations where radii of the ${}^6\text{Li}$ and ${}^6\text{He}$ g.s. are practically equal to the radius of the 3.56 MeV state [18].

V. CONCLUSION

${}^7\text{Li}$ elastic scattering and the lithium-induced reaction of one-nucleon transfers from ${}^{10}\text{B}({}^7\text{Li}, {}^6\text{Li}){}^{11}\text{B}$ has been measured at $E_{\text{LAB}}({}^7\text{Li}) = 58$ MeV. Experiment was done at the U-400 accelerator beam of the FLNR JINR, Dubna. Angular distributions for the ground and the 3.56 MeV excited states of the ${}^6\text{Li}$ were measured in the lab angular range $\Theta_{\text{LAB}} = (7^\circ - 50^\circ)$. Angular distribution for the ${}^6\text{Li}(J^\pi = 0^+, T = 1, E = 3.56 \text{ MeV})$ state are presented for the first time.

The DWBA analysis of the differential cross section of the ${}^{10}\text{B}({}^7\text{Li}, {}^6\text{Li}){}^{11}\text{B}$ reaction with excitation of the ${}^6\text{Li}_{\text{g.s.}}$ and the

${}^6\text{Li}(J^\pi = 0^+, T = 1, E = 3.56 \text{ MeV})$ states was performed. The use of DWBA in the region of the main peak of the angular distribution is quite adequate, since the reaction is direct and peripheral and allows obtaining information about the interactions and structure of the participating nuclei. As a first step of analysis, optical model potentials were obtained by fitting measured elastic scattering data and evaluating optical potential parameters for the output reaction channels. Using a minimum number of variable parameters, we have obtained the correct energy behavior of the potential characteristics and a fairly good description of the data in the region of forward angles.

Phenomenological approach based on solving an approximate equation for the form factor was used to determine radial dependence of the reaction form factor. As reaction is peripheral, the angular distributions are sensitive only to the surface (asymptotic) part of the reaction form factor. This allowed us to obtain empirical values of ANC (and NVC). We obtain radial dependences of the form factors and the ANC values for ${}^6\text{Li}_{\text{g.s.}}$ and ${}^6\text{Li}(J^\pi = 0^+, T = 1, E = 3.56 \text{ MeV})$ states. Obtained values of ANC's for ${}^6\text{Li}_{\text{g.s.}}$ and ${}^6\text{Li}(J^\pi = 0^+, T = 1, E = 3.56 \text{ MeV})$ states are similar to literature one. This fact confirms correctness of our DWBA analysis. Comparison of the radial dependences of form factors shows that the wave function of the ${}^6\text{Li}$ nucleus in the ${}^6\text{Li}(J^\pi = 0^+, T = 1, E = 3.56 \text{ MeV})$ state has increased spatial dimension compared to the ${}^6\text{Li}_{\text{g.s.}}$ state, and in both cases some larger spatial size than the ground states of the ${}^{11}\text{B}$ and ${}^{10}\text{B}$. Within the framework of our analysis, we can confirm that the radius of the ${}^6\text{Li}$ nucleus in the 3.56 MeV state is larger than in the ground state. This result is an argument in favor of a halo existence in ${}^6\text{Li}^*(3.56 \text{ MeV})$ state, while the question of a halo in ${}^6\text{Li}_{\text{g.s.}}$ still leaves open.

[1] I. Tanihata, H. Hamagaki, O. Hashimoto, *et al.*, Physical Review Letters, 55(24):2676–2679 (1985). DOI: <https://doi.org/10.1103/PhysRevLett.55.2676>

[2] K Riisager, Physica Scripta, T152:014001 (2013). DOI: <https://doi.org/10.1088/0031-8949/2013/t152/014001>

- [3] Igor Izosimov, EPJ Web of Conferences, 107:09003 (2016). DOI: <https://doi.org/10.1051/epjconf/201610709003>
- [4] I. N. Izosimov, Physics of Atomic Nuclei, 80(5):867–876 (2017). DOI: <https://doi.org/10.1134/S1063778817050118>
- [5] I. N. Izosimov, Physics of Particles and Nuclei Letters, 15(6):621–626 (2018). DOI: <https://doi.org/10.1134/S1547477118060092>
- [6] Igor Izosimov, EPJ Web of Conferences, 239:02003 (2020). DOI: <https://doi.org/10.1051/epjconf/202023902003>
- [7] Yu Sobolev, A. Budzanowski, E. Bialkowski, *et al.*, Bulletin of The Russian Academy of Sciences: Physics, 69:1790–1795 (2005).
- [8] Konstantin Lukyanov, Elena Zemlyanaya, V. Lukyanov, *et al.*, Bulletin of The Russian Academy of Sciences: Physics, 72:356–360 (2008). DOI: <https://doi.org/10.3103/s11954-008-3019-7>
- [9] R. Kalpakchieva, V. A. Maslov, R. A. Astabatian, *et al.*, Physics of Atomic Nuclei, 70(4):619–625 (2007). DOI: <https://doi.org/10.1134/S1063778807040023>
- [10] M.D. Cortina-Gil, P. Roussel-Chomaz, N. Alamanos, *et al.*, Physics Letters B, 371(1–2):14–18 (1996). DOI: [https://doi.org/10.1016/0370-2693\(95\)01582-5](https://doi.org/10.1016/0370-2693(95)01582-5)
- [11] M.D. Cortina-Gil, A. Pakou, N. Alamanos, *et al.*, Nuclear Physics A, 641(3):263–270 (1998). DOI: [https://doi.org/10.1016/S0375-9474\(98\)00470-9](https://doi.org/10.1016/S0375-9474(98)00470-9)
- [12] J. A. Brown, D. Bazin, W. Benenson, *et al.*, Physical Review C, 54(5):R2105–R2108 (1996). DOI: <https://doi.org/10.1103/physrevc.54.r2105>
- [13] Zhihong Li, Weiping Liu, Xixiang Bai, *et al.*, Physics Letters B, 527(1–2):50–54 (2002). DOI: [https://doi.org/10.1016/S0370-2693\(02\)01172-3](https://doi.org/10.1016/S0370-2693(02)01172-3)
- [14] L. I. Galanina and N. S. Zelenskaya. Physics of Atomic Nuclei, 77(6):704–715 (2014). DOI: <https://doi.org/10.1134/S106377881405007x>
- [15] A S Demyanova, A A Ogloblin, A N Danilov, *et al.*, KnE Energy, 3(1):1, (2018). DOI: <https://doi.org/10.18502/ken.v3i1.1715>
- [16] A. N. Danilov, T. L. Belyaeva, A. S. Demyanova, *et al.*, Physical Review C, 80(5):054603 (2009). DOI: <https://doi.org/10.1103/physrevc.80.054603>
- [17] R.W. Givens, M.K. Brussel, and A.I. Yavin. Nuclear Physics A, 187(3):490–500 (1972). DOI: [https://doi.org/10.1016/0375-9474\(72\)90674-4](https://doi.org/10.1016/0375-9474(72)90674-4)
- [18] D. M. Rodkin and Yu. M. Tchuvil'sky. JETP Letters, 118(3):153–159 (2023). DOI: <https://doi.org/10.1134/S0021364023602130>
- [19] I. Tanihata, H. Hamagaki, O. Hashimoto, 054603 Physical Review Letters, 55(24):2676–2679 (1985). DOI: <https://doi.org/10.1103/physrevlett.55.2676>
- [20] A.V. Dobrovolsky, G.D. Alkhazov, M.N. Andronenko, *et al.*, Nuclear Physics A, 766:1–24 (2006). DOI: <https://doi.org/10.1016/j.nuclphysa.2005.11.016>
- [21] A. Etchegoyen, M. C. Etchegoyen, E. D. Izquierdo, *et al.*, Physical Review C, 38(5):2124–2133 (1988). DOI: <https://doi.org/10.1103/physrevc.38.2124>
- [22] P. Schumacher, N. Ueta, H.H. Duhm, *et al.*, Nuclear Physics A, 212(3):573–599 (1973). DOI: [https://doi.org/10.1016/0375-9474\(73\)90824-5](https://doi.org/10.1016/0375-9474(73)90824-5)
- [23] Detector readout systems. <http://www.mesytec.com/>. Accessed: 2024-08-15.
- [24] G R Satchler. *Direct Nuclear Reactions*. International Series of Monographs on Physics. Clarendon Press, Oxford, England, 1983.
- [25] E. Bang, V. E. Bunakov, F. A. Gareev *et al.*, Fiz. Elem. Chast. Atom. Yadra, 5:263–307, (1974).
- [26] L. Blokhintsev, I. Borbely, and E.I. Dolinskii. Sov. J. Particles Nucl, 8(11):1189 (1977).
- [27] S.A. Goncharov, J. Dobesh, E.I. Dolinskii *et al.*, Sov. J. Nucl. Phys., 35(3) (1982).
- [28] Ian J. Thompson. Computer Physics Reports, 7(4):167–212 (1988). DOI: [https://doi.org/10.1016/0167-7977\(88\)90005-6](https://doi.org/10.1016/0167-7977(88)90005-6)
- [29] B.Ja. Guzhovskij, S.N. Abramovich, B.M. Dzuba *et al.*, Problemy Yadernoj Fiziki i Kosmicheskikh Luchejs, 7:41 (1977).
- [30] J. D. Sherman, E. R. Flynn, Nelson Stein *et al.*, Physical Review C, 13(6):2122–2126 (1976). DOI: <https://doi.org/10.1103/PhysRevC.13.2122>
- [31] P. L. Kerr, K. W. Kemper, P. V. Green *et al.*, Physical Review C, 52(4):1924–1933 (1995). DOI: <https://doi.org/10.1103/physrevc.52.1924>
- [32] A.S. Demyanova et al. Dimensions of ^6Li in low-lying states. In *Proceedings of the LXXIV International conference "NUCLEUS-2024, Fundamental problems and applications"* Dubna, July 1-5, page 155 (2024).
- [33] I. Gulamov, Akram Mukhamedzhanov, and G. Nie, Physics of Atomic Nuclei, 58:1689–1695 (1995).
- [34] N. K. Timofeyuk. Physical Review C, 81(6):064306 (2010). DOI: <https://doi.org/10.1103/physrevc.81.064306>
- [35] W. Kohler, G. Gruber, A. Steinhauser *et al.*, Nuclear Physics A, 290(1):233–252 (1977). DOI: [https://doi.org/10.1016/0375-9474\(77\)90677-7](https://doi.org/10.1016/0375-9474(77)90677-7)

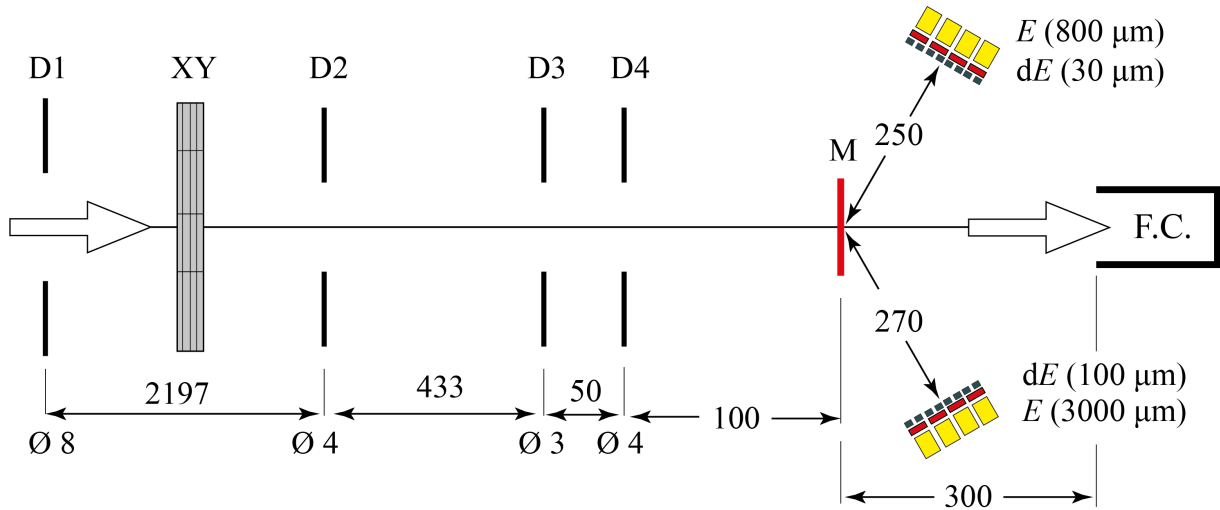


Fig. 1. Schematic view diagram of the experimental setup for measuring differential cross sections of the ${}^7\text{Li}+{}^{10}\text{B}$ reaction products. The values of diameters and distances between the setup elements are given in millimeters.

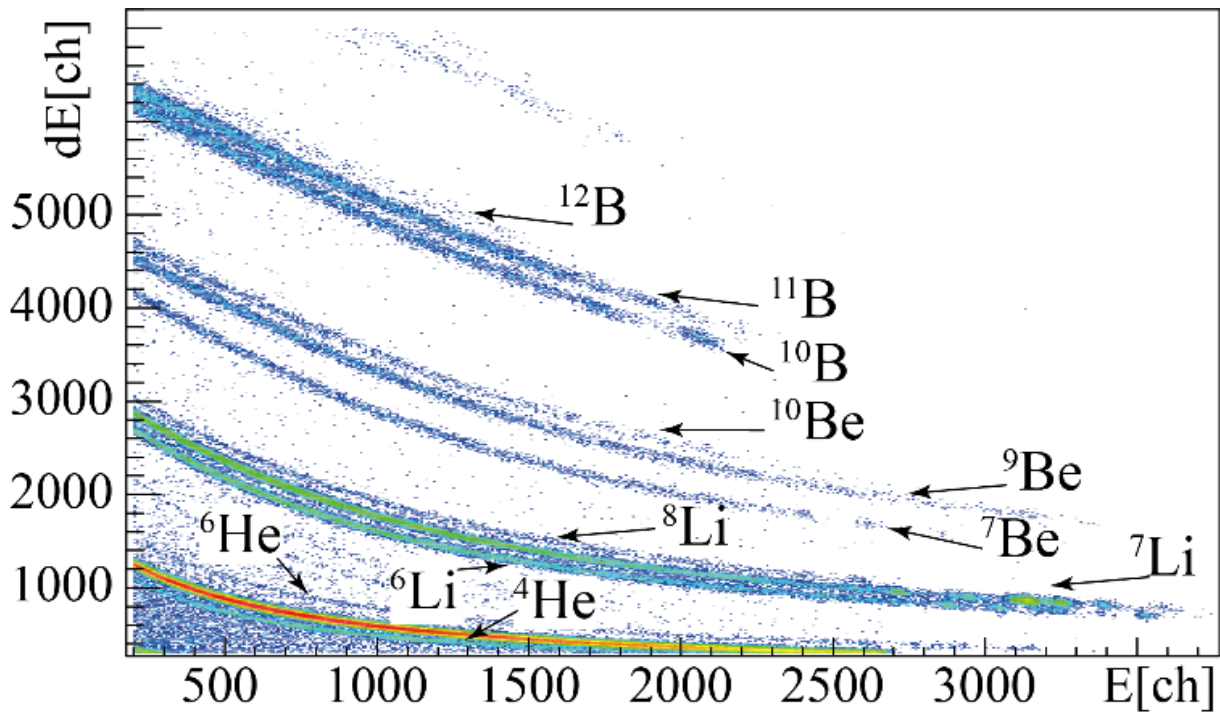


Fig. 2. Two-dimensional $\Delta E \times E$ spectrum of reaction products ${}^7\text{Li}+{}^{10}\text{B}$.

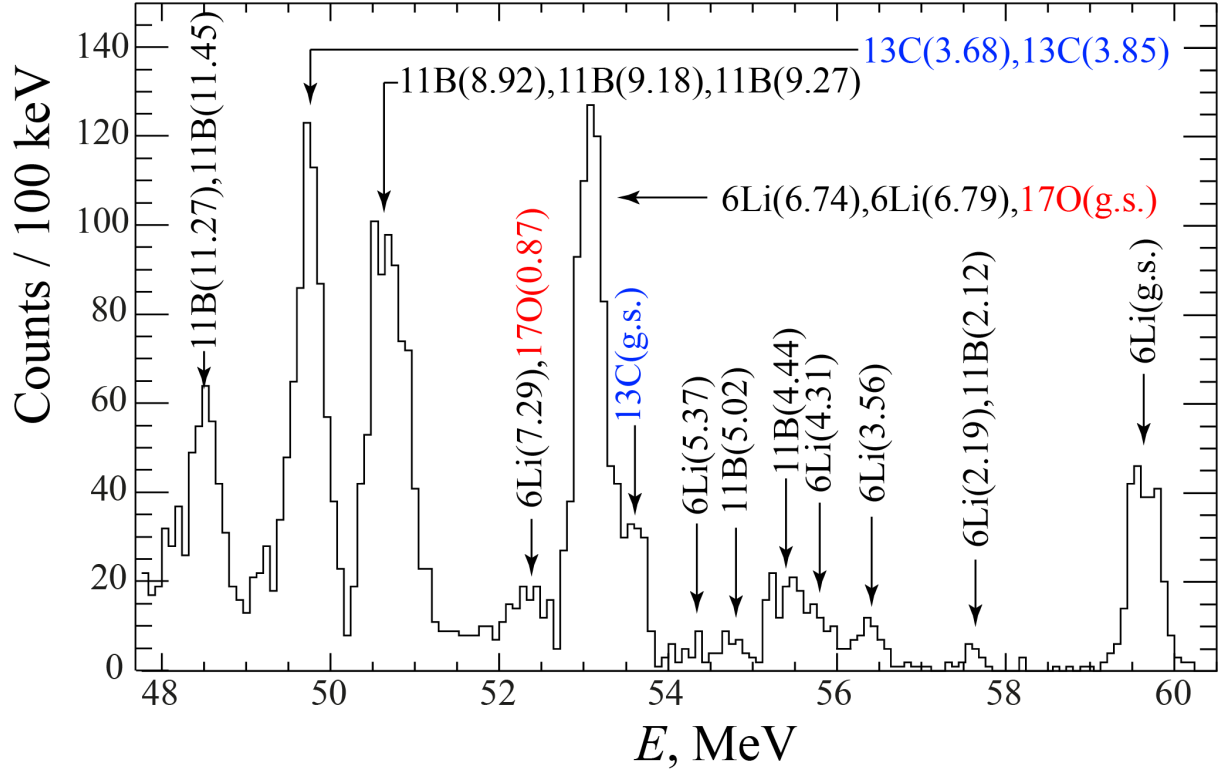


Fig. 3. Energy ($\Delta E + E$) spectrum of ${}^6\text{Li}$ recorded at $\Theta_{\text{LAB}} = 10^\circ$. Black color indicates the ${}^6\text{Li}$ peaks from the reaction on the ${}^{10}\text{B}$ target, blue and red indicate the ${}^6\text{Li}$ peaks obtained in reactions on ${}^{12}\text{C}$ and ${}^{16}\text{O}$ impurities, respectively

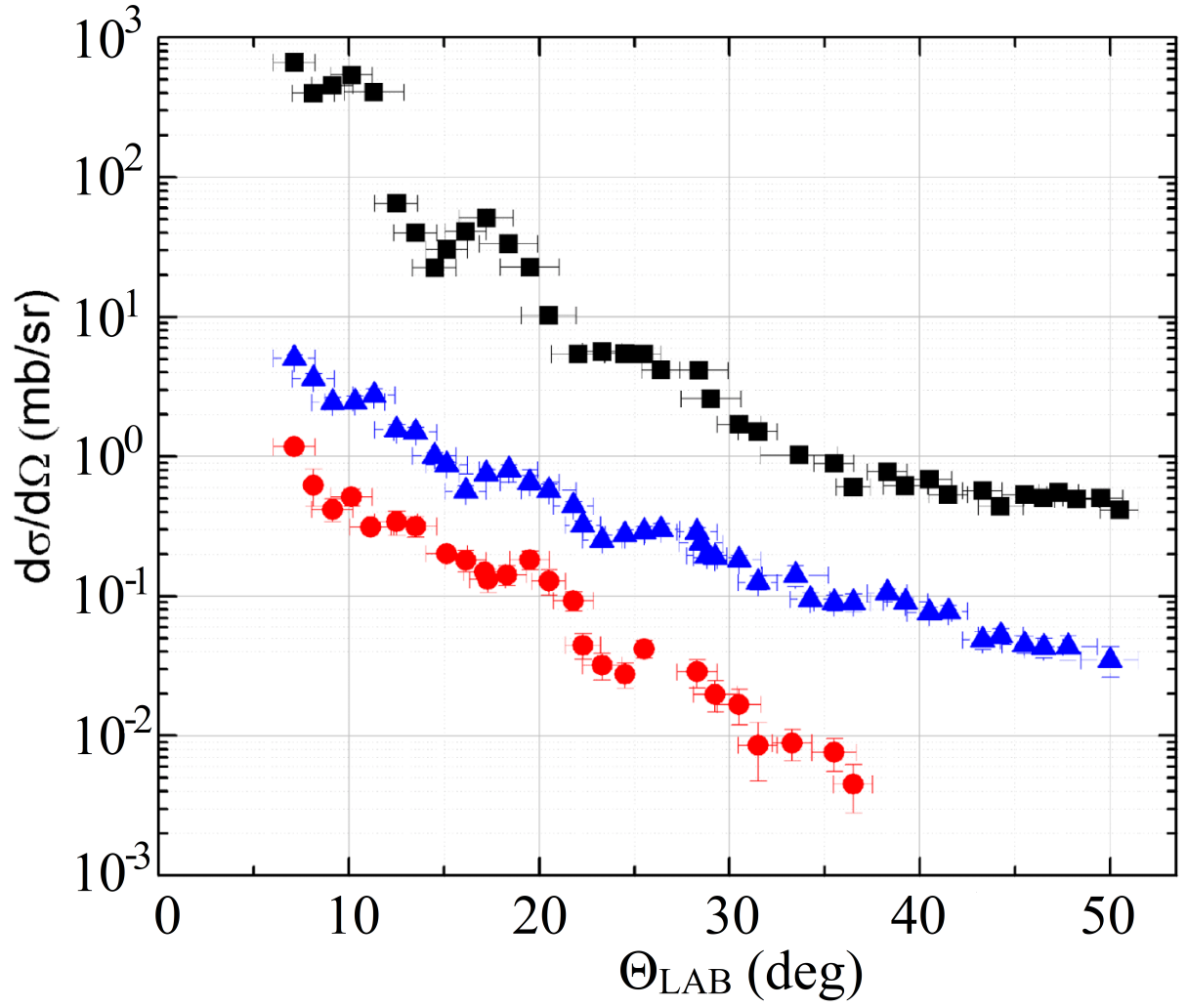


Fig. 4. Angular distributions of differential cross sections of elastic scattering of (${}^7\text{Li}+{}^{10}\text{B}$) and reaction channels of transfer ${}^{10}\text{B}({}^7\text{Li}, {}^6\text{Li}){}^{11}\text{B}$ to the ground ${}^6\text{Li}$ and excited ${}^6\text{Li}(J^\pi = 0^+, T = 1, E = 3.56 \text{ MeV})$ states of ${}^6\text{Li}$. Black squares correspond to elastic scattering of ${}^7\text{Li}+{}^{10}\text{B}$, blue triangles to the ground state of ${}^6\text{Li}_{\text{g.s.}}$, red circles to the excited state of ${}^6\text{Li}(J^\pi = 0^+, T = 1, E = 3.56 \text{ MeV})$.

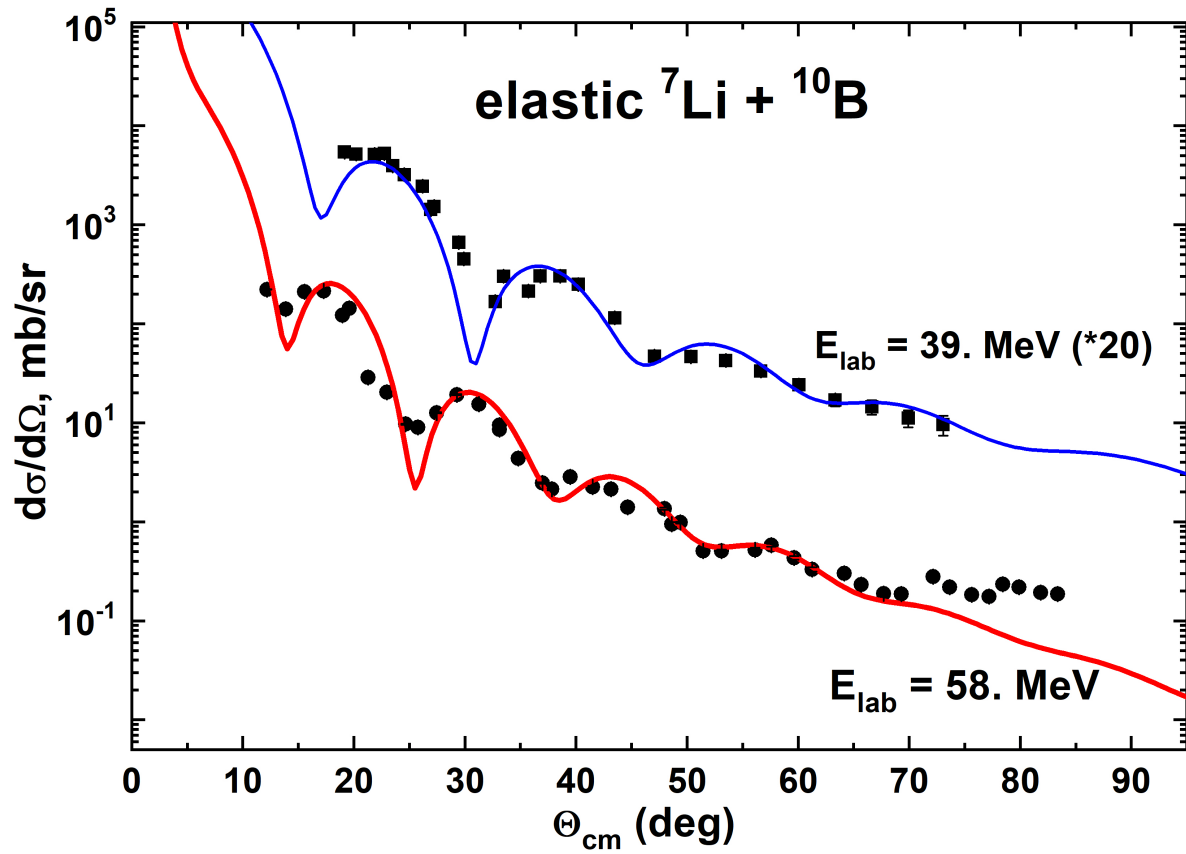


Fig. 5. Differential cross sections of elastic scattering ${}^7\text{Li} + {}^{10}\text{B}$ at energies of 58 and 39 MeV are presented. Black circles and squares are experimental data, solid lines are calculations with the obtained optical potentials

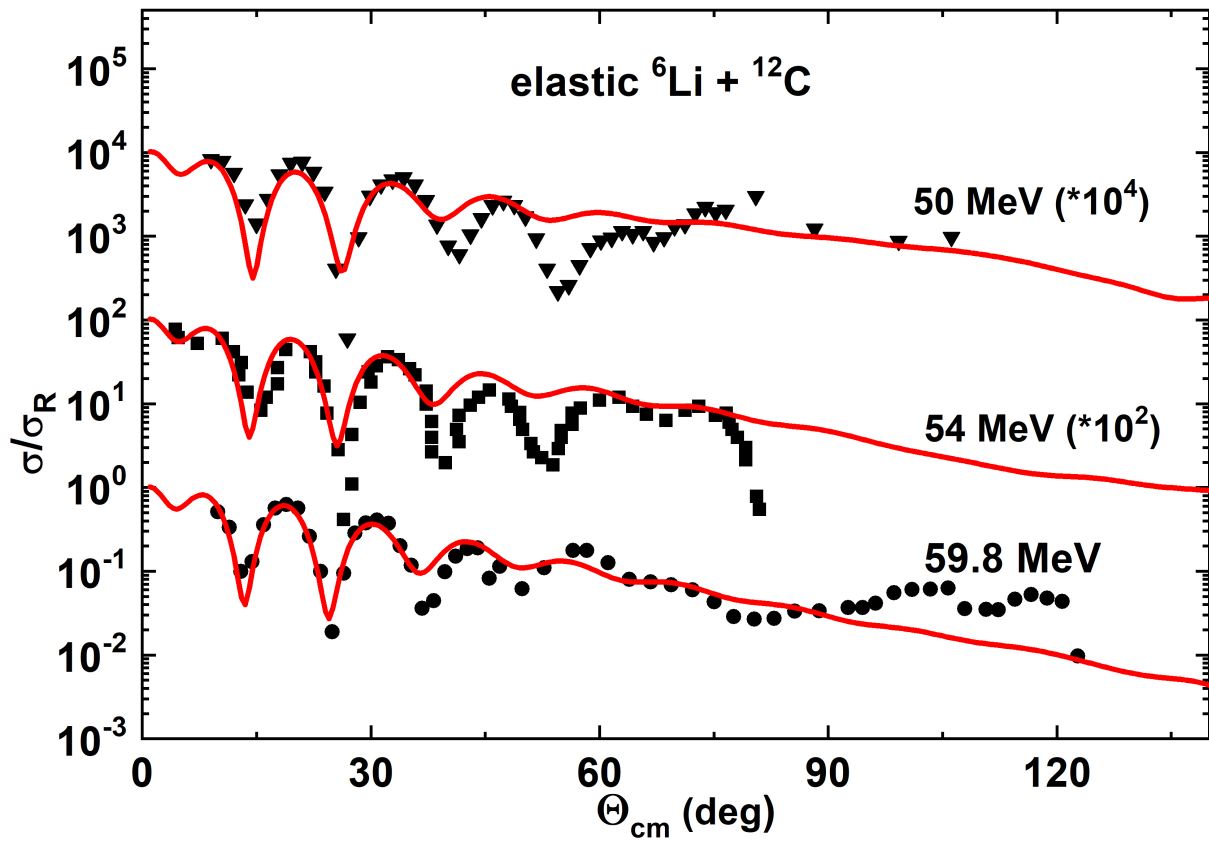


Fig. 6. Differential cross sections of elastic scattering ${}^6\text{Li}+{}^{12}\text{C}$ at energies of 50, 54 and 59.8 MeV are present. Black circles, triangles and squares are experimental data [29–31], solid lines are calculations with the obtained optical potentials

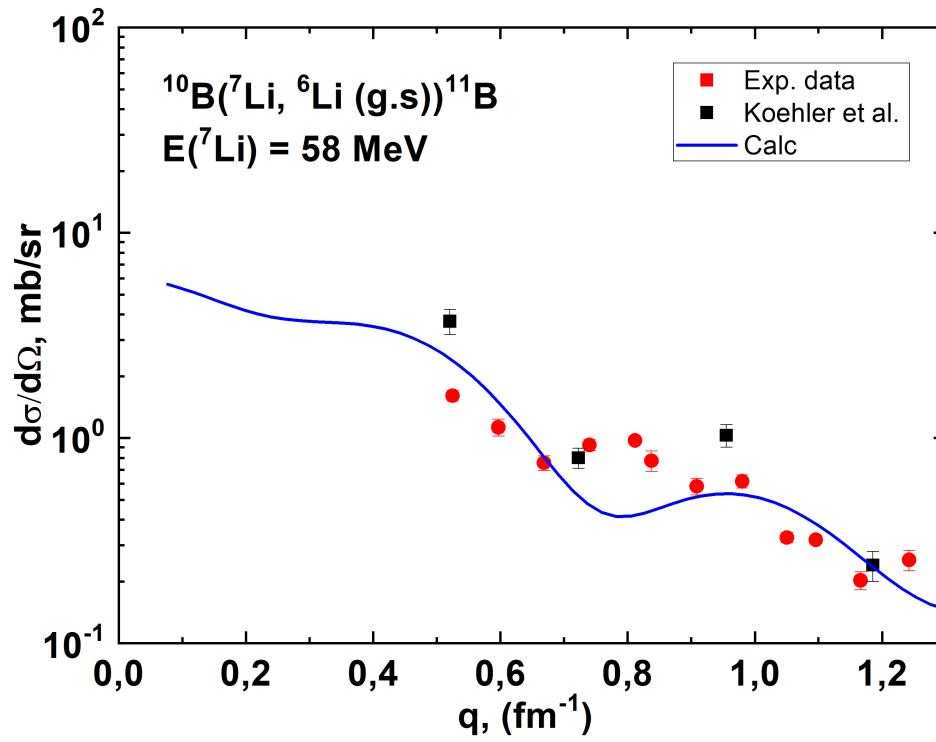


Fig. 7. Differential cross sections of the reaction $^{10}\text{B}(^7\text{Li}, ^6\text{Li})^{11}\text{B}$ for ground state of ^6Li . Red circles – our data at 58 MeV, squares – data at 24 MeV from [35], solid line – the DWBA calculations.

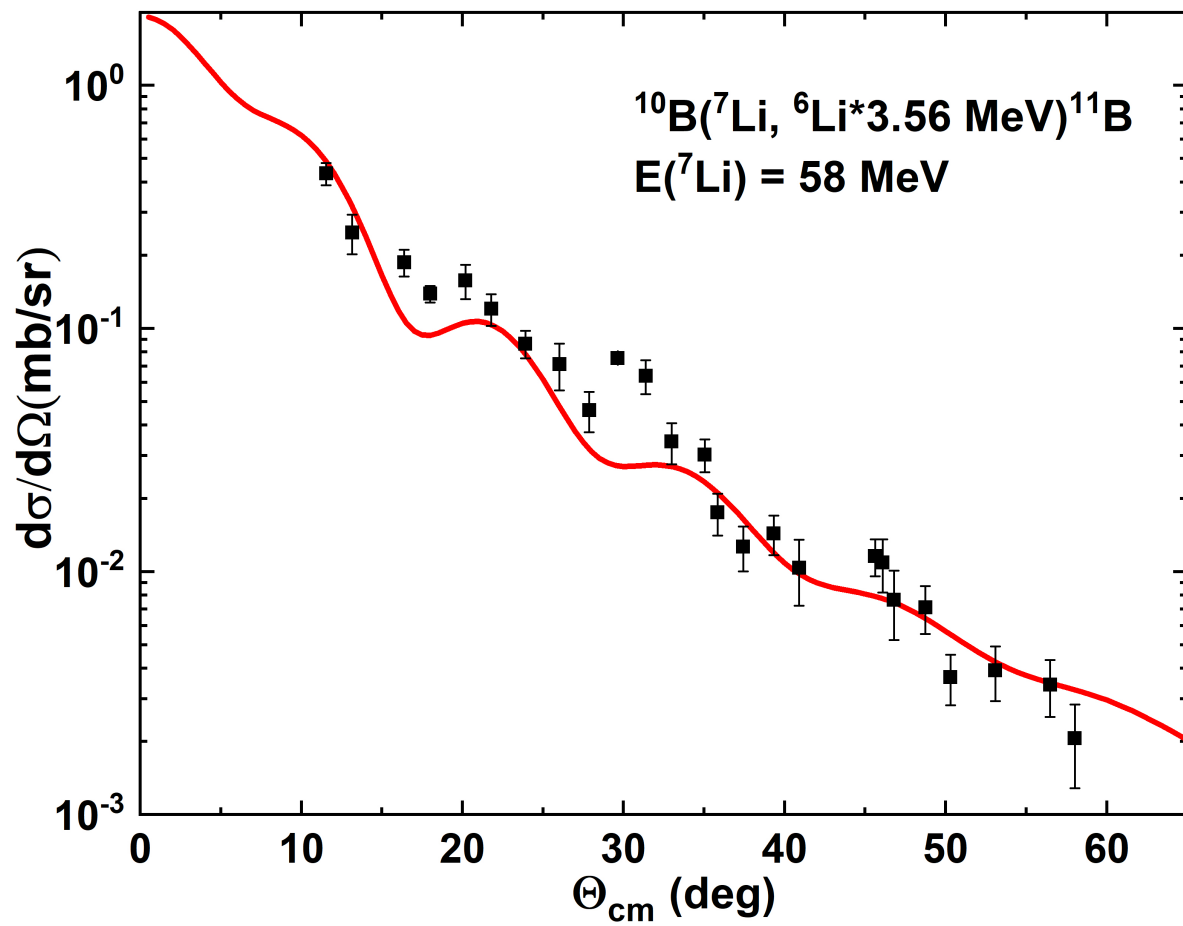


Fig. 8. Differential cross sections of the reaction $^{10}\text{B}(^7\text{Li}, ^6\text{Li}^*3.56 \text{ MeV})^{11}\text{B}$ at 58 MeV with excitation of the 3.56 MeV state of ^6Li . Black circles are experimental data, solid lines are the DWBA calculations

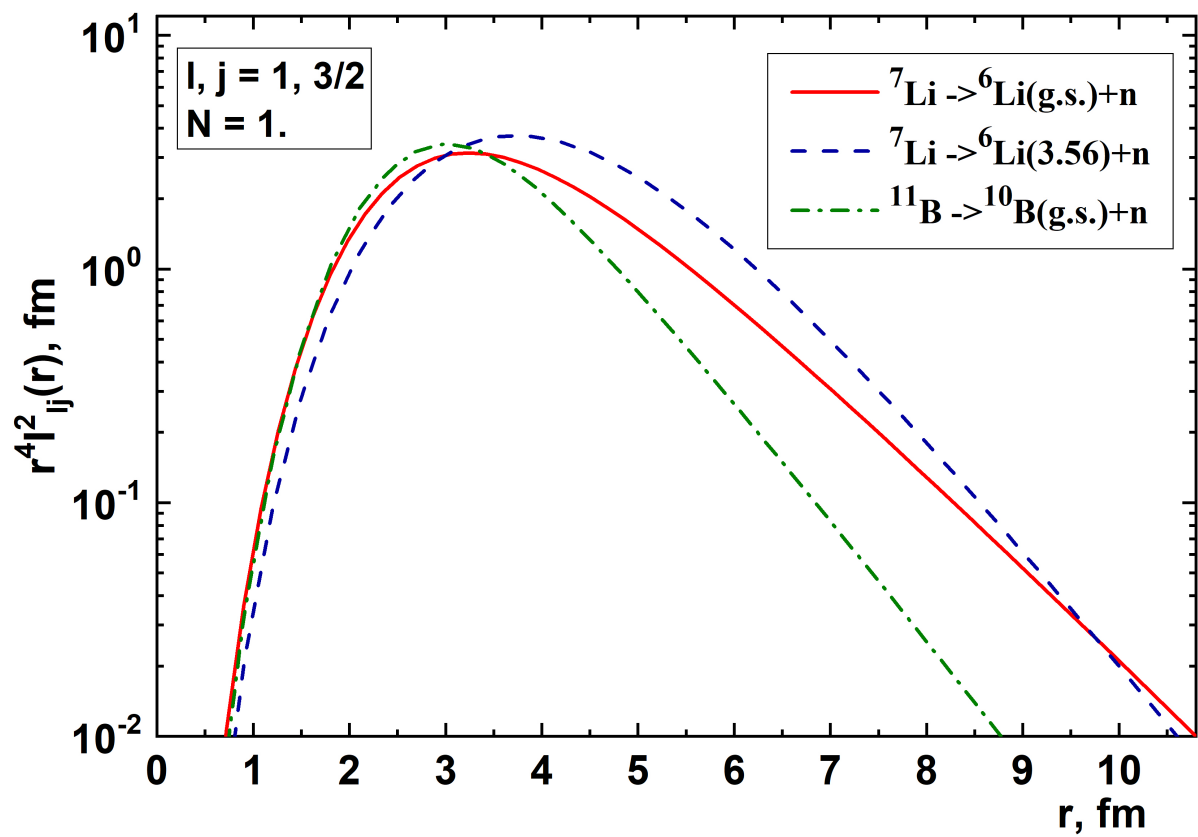


Fig. 9. Comparison of the radial dependences of the values $r^4 I_{ij}^2(r)$ for all three form factors